MECSOL Joinville 2017

April 26-28, 2017
Joinville, Santa Catarina, Brazil

Proper Generalized Decomposition (PGD) representation of highly heterogeneous material property in a Representative Volumetric Element

Paulo de Tarso R Mendonça
Department of Mechanical Engineering
Federal University of Santa Catarina
mendonca@grante.ufsc.br

Clovis S. de Barcellos
Department of Mechanical Engineering
Federal University of Santa Catarina
clovis.barcellos@gmail.com

Leonardo K. Granemann
Department of Mechanical Engineering
Federal University of Santa Catarina
leonardo.k.granemann@gmail.com

ABSTRACT

The first part of this research describes an attempt to develop a formulation to obtain 3D approximate solutions for the heat conduction problem in highly heterogeneous materials, by a sequence of one-dimensional FEM problems generated by the Proper Generalized Decomposition (PGD) technique. Here only the steady state problem is considered. Along the PGD iterations, the separation of variables is done between the all three space coordinates, instead of the time as it is usual in PGD applications. In this way, it is sought to obtain, iteratively, an accurate a-posteriori approximation of the complex oscillation of the temperature, with a reduced number of modes.

The method involves an iterative sequence of global solutions, even in a linear problem. However, previous experiences in the literature shows that the number of iterations and modes is small, and the total computational cost involved is generally smaller than the cost of the single 3D analysis by 3D solid finite elements model. Also, if the process converges adequately, it is expected that an accurate 3D solution can be well estimated in boundary layers and other regions with high gradients in the solution.

Formulations for three complementary problems are developed. Firstly, a procedure to generate data for a material property, for example thermal conductivity, is commented, in the frame of randomly distributed inclusions on a material matrix, generating a highly oscillating function of the local property over the domain.

Second, a PGD formulation is developed to obtain a PGD description of a highly oscillatory local material property data. This description is composed by a sequence of discrete modes uncoupled in each of the three Cartesian coordinates, and are used in the third formulation. The third formulation is a homogenization problem for the heat conduction problem, where the PGD formulation is applied in a regular representative volume to obtain the homogenized thermal conductivity tensor of the material. All data (material property, heat source and Dirichlet and Neumann boundary condition functions) are represented by their adequate PGD modes.

Keywords: Proper Orthogonal Decomposition, Tensor product

1. INTRODUCTION

Along the last decades, the constitutive modeling in solids have concentrated with two large families of methods, the multi-scale and homogenization ones. Among the classic works one can reference [1–11].

In some fields like rock mechanics, one of the principal methods used to mechanical characterization use samples of the material extracted from the region of interest in the soil, or oil reservoir [12]. The samples are removed from different positions of the field, at regular intervals, and from then specimens are extracted, called *plugs*. The plugs are tested and the results generate an estimate of the properties variation in the field. However, the tests are expensive, take time and need specialized personal. Thus, in the last years, the techniques of analysis of digitalized images has gained preference, because of lower costs involved. The images are obtained from the samples with a technique of microtomography, which produces a tridimensional representation of the sample [13]. With the geometric representation, it is possible to perform numerical simulations and obtain, for example, homogeneous properties of the rock properties.

The homogenized properties at a point in the body are obtained by procedures that identify an average value of the same property in the macroscale, and it is expected it represents the physical response at the point considered. The need for the averaged properties is essential in multiphase materials, natural or artificials. Each phase presents different values for the property and occupies a given region in space, with characteristic size and shape in the microscale. The relative dimension of the phase in general is several orders of magnitude smaller than the body size.

The classic formulation in solid mechanics, used in works of, for example, [14–16], are based in a boundary value problem. The procedure consists, in short, in identifying a Representative Volume Element, RVE, whose dimensions must be adequate to include a representative microstructure of the material. Then, numerical tests are performed to obtain an homogeneous values of the required properties.

Even though the homogezation strategies have become almost routine, there are still many limitations in terms of computational cost. Let us consider the usual processing of a digitalized sample, in a discretization of 600^3 voxels, each voxel represents a cube of side 5,6 μm, generating a cube with side 3360 μm. Considering a numerical thermal or mechanical analysis, by the finite element method, a mesh which can be considered viable to be solved with a reasonable computation time in a common computer can have between 30 and 100 elements along each direction. This means about 30^3 a 100^3 elements, that is, between 27000 and a million three dimensional finite elements. However, the order of magnitude of the geometry captured in the microthomography is much finer, and needs a quantity of information of 600 values by direction. A finite element mesh adequate to model this geometry would need a similar number of elements of the digital image, that is, $600^3 = 216$ million of nodes, which is, nowadays, impossible in a routine analysis.

Two procedures are commonly used in the finite element analysis. The first is the use of one or more levels of multi-scale analysis of the sample. The other procedure is by the use of a mesh with a viable density, such that each element has a quantity of voxels. Each voxel has associated a property value, form example 0 and 1 in a two phase material. One can, for example, attribute a property 0 (or 1), if the density of 0 (or 1) in the voxels inside the element is more than 50 %. This is equivalent to the famous mixture rule [17].

The use of PGD in the analysis of the RVE is a more recent and promising family of technique to deal with the problem. It is one of the few methods capable to challenge the so called *curse of dimensionality*. This curse is the exponential growth of the number of degrees of freedom in a numerical model with the growth of the number of dimensions of the problem. In the present case, the same accuracy that could usually be obtained only in a 2 D problem, becomes viable in three or

more dimensions using PGD.

The basic mathematical structure of the formulation is described in section 2. Some basic references are seen in [18–20] for the separation of variables in space, time, geometric parameters or material properties. With this, we seek to be able to model a sample with the a grid of the same refinement of the digitalized image, that is, advance from the approximately 100 elements by direction in the sample, to about 600. As important as this, the development makes viable the modeling of larger samples, which gives more representativity to the sample. The main focus of the present paper is developed in section 3. and consists in the obtaining PGD representation of local properties in a RVE, processing digitalized data obtained from any experimental process. As seen in section 2. this is an essential requirement in the application of PGD method to the problem of heat transfer itself in the RVE.

2. PGD in space for the heat conduction problem

Let us initially consider a body subject to adequate source load and boundary conditions, with the geometric form of a regular volume Ω with dimensions $\Omega = L_x \times L_y \times L_z$ along the Cartesian coordinates $x = (x, y, z)$. The boundary Γ of the body is composed by the six faces, f_1 to f_6, designated as Γ_1, Γ_2, $\cdots$, Γ_6, where Γ_1 and Γ_2 have normals oriented along $-x$, $+x$, Γ_3 and Γ_4 normals along $-y$, $+y$ axis, respectively, and similarly for Γ_5 and Γ_6. The coordinates of the faces $f = 1$ and 2 are $x_f = 0$ and L_x, for faces $f = 3$ and 4 the coordinates are $y_f = 0$ and L_y. Here we consider the strong form for homogeneous and isotropic material, and steady state heat flux:

$$\begin{aligned} k\nabla^2\theta &= -b, \quad \text{that is,} \quad kT_{,jj} = -b \qquad \text{(summation rule)} \\ \theta(x) &= \bar{T}(x) \quad \text{for } x \in \Gamma_u, \\ q &= k\nabla T = h(x) \quad \text{for } x \in \Gamma_q, \end{aligned} \tag{1}$$

where $\bar{T}(x)$ and h are temperature and heat flux prescribed on parts of the boundary. We consider a decomposition of the temperature field as

$$\begin{aligned} \theta(x) &= T(x) + G(x), \text{ for } x \in \Omega, \text{ where} \\ T(x) &= 0 \qquad \text{for } x \in \Gamma_u, \\ G(x) &= \bar{T}(x), \qquad \text{for } x \in \Gamma_u, \end{aligned} \tag{2}$$

The decomposition generates the following weak form: given $G \in Kin$, *find* $T \in Var$

$$\int_\Omega \nabla\hat{u} \cdot (k\nabla T)\ d\Omega = \int_\Omega \hat{u}b\ d\Omega + \int_{\Gamma_q} \hat{u}h\ d\Gamma - \int_\Omega \nabla\hat{u} \cdot (k\nabla G)\ d\Omega, \quad \text{for } \forall\hat{u} \in Var, \tag{3}$$

where the sets of solution and of variations are the same:

$$Kin = Var = \left\{ f \in H^1(\Omega), \text{ such that } f(x) = 0 \text{ for all } x \in \Gamma_u \right\}. \tag{4}$$

Consider available the PGD representation of $k(x)$ and $b(x)$,

$$\begin{aligned} b(x) &= \sum_{j=1}^{nb} L_j b_{xj}(x) b_{yj}(y) b_{zj}(z), \\ k(x) &= \sum_{l=1}^{nk} D_l k_{xl}(x) k_{yl}(y) k_{zl}(z), \end{aligned} \tag{5}$$

and consider also the PGD representation of the prescribed temperature and heat flux at the six faces, $f = 1,2,...,6$, of the boundaries:

$$\begin{aligned} \bar{T}_f(x) &= \delta_{Tf} \sum_{s=1}^{ns} J_s G_{fxs}(x) G_{fys}(y) G_{fzs}(z), \\ h_f(x) &= \delta_{hf} \sum_{r=1}^{nh} H_r h_{fxr}(x) h_{fyr}(y) h_{fzr}(z), \end{aligned} \tag{6}$$

$\delta_{Tf} = 1$ if $\Gamma_f \in \Gamma_u$ and $\delta_{Tf} = 0$ otherwise. $\delta_{hf} = 1$ if $\Gamma_f \in \Gamma_q$ and $\delta_{hf} = 0$ otherwise. One observe that, since each face is orthogonal to one of the Cartesian directions, in each face of the representations (6) one of the functions are absent. For example, if face $f = 1$ has prescribed temperature, $T_{fxp}(x) = 1$, and $\bar{T}_f(x)$ depends only on (y,z). In general, if $f = 1$ or 2, $G_{fxs}(x) = h_{fxr}(x) = 1$. If $f = 3$ or 4, $G_{fys}(x) = h_{fyr}(x) = 1$.

Let us consider that there are already available *nu* PGD modes, and we seek the next mode $T_{nu+1}(x)$. Thus, we have the following representation with variation separation:

$$T(x) = \underbrace{\sum_{m=1}^{nu} T_{xm}(x) T_{ym}(y) T_{zm}(z)}_{T_0(x)} + \underbrace{T_x(x) T_y(y) T_z(z)}_{T_{nu+1}(x)}, \quad \text{that is, } T(x) = T_0(x) + T_{nu+1}(x). \tag{7}$$

where $T_0(x)$ is known and we seek $T_{nu+1}(x)$. We proceed to a **spatial discretization** of $T_n(x)$:

$$\begin{aligned} T_x(x) &= \sum_{p=1}^{px} T_{xp} \phi_{xp}(x) = \Phi_x(x) T_x, \quad \text{for } x \in [0, L_x], \\ T_y(y) &= \sum_{p=1}^{py} T_{yp} \phi_{yp}(y) = \Phi_y(y) T_y, \quad \text{for } y \in [0, L_y], \\ T_z(z) &= \sum_{p=1}^{pz} T_{zp} \phi_{zp}(z) = \Phi_z(z) T_z, \quad \text{for } z \in [0, L_z]. \end{aligned} \tag{8}$$

These functions must satisfy:

$$T_x(x) \in Var_x, \quad T_y(y) \in Var_y, \quad T_z(z) \in Var_z,$$

where the spaces are:

$$\begin{aligned} Var_x &= \left\{ f \in H^1(\Omega_x), \text{ such that } f(x) = 0 \text{ for all } x \in \Gamma_x \right\}, \\ Var_y &= \left\{ f \in H^1(\Omega_y), \text{ such that } f(y) = 0 \text{ for all } y \in \Gamma_y \right\}, \\ Var_z &= \left\{ f \in H^1(\Omega_z), \text{ such that } f(z) = 0 \text{ for all } z \in \Gamma_z \right\}. \end{aligned} \tag{9}$$

$\Omega_x = (0, L_x)$ and $\Gamma_x = \{0, L_x\}$ are the domain in the x dimension and its boundary. Similarly for Ω_y, Ω_z, Γ_y and Γ_z. Each set of functions $\phi_{xp}(x)$, etc is a set of piecewise continuous finite element basis functions, one-dimensional, associated with a given mesh, and T_x, T_y etc, are unknown nodal coefficients for the n-th PGD mode of the temperature. In the present formulation, $T_x(x) \in Var_x$ but

not all basis component $\phi_{xp}(x)$ are required to belong to Var_x. Nodes p span the entire domain $\bar{\Omega}_x$. Thus, the condition $T_x(x) = 0$ on $x \in \Gamma_x$ is satisfied adjusting the adequate nodal value in T_x and in its variation $\hat{T}_x$. The same holds for $\phi_{yp}(y)$ and $\phi_{zp}(z)$.

The temperature gradient is discretized by

$$\begin{aligned} \nabla T &= \nabla T_0 + \nabla T_n, \text{ i.e.,} \\ \nabla T &= \nabla T_0 + \left\{ \begin{array}{l} (\Phi_{x,x} T_x)(\Phi_y T_y)(\Phi_z T_z) \\ (\Phi_x T_x)(\Phi_{y,y} T_y)(\Phi_z T_z) \\ (\Phi_x T_x)(\Phi_y T_y)(\Phi_{z,z} T_z) \end{array} \right\}. \end{aligned} \tag{10}$$

The variation of the temperature is

$$\hat{T}(x) = \hat{T}_n(x) = \hat{T}_x T_y T_z + T_x \hat{T}_y T_z + T_x T_y \hat{T}_z, \tag{11}$$

Taking the variations separately we have the following cases.
Case I - only $\hat{T}_x \neq 0$, that is, $\hat{T}_y = \hat{T}_z = 0$. From (11),

$$\begin{aligned} \hat{T}(x) &= \hat{T}_n(x) = \hat{T}_x T_y T_z = [T_y T_z \Phi_x]_{1 \times P_x} \hat{T}_x = N_x \hat{T}_x, \\ \delta \nabla T &= \left[\begin{array}{c} T_y T_z \Phi_{x,x} \\ T_{y,y} T_z \Phi_x \\ T_y T_{z,z} \Phi_x \end{array} \right]_{3 \times P_x} \hat{T}_x = B_x \hat{T}_x. \end{aligned} \tag{12}$$

Case II - only $\hat{T}_y \neq 0$, that is, $\hat{T}_x = \hat{T}_z = 0$. From (11),

$$\begin{aligned} \hat{T}(x) &= \hat{T}_n(x) = T_x \hat{T}_y T_z = [T_x T_z \Phi_y]_{1 \times P_y} \hat{T}_y = N_y \hat{T}_y, \\ \delta \nabla T &= \left[\begin{array}{c} T_{x,x} T_z \Phi_y \\ T_x T_z \Phi_{y,y} \\ T_x T_{z,z} \Phi_y \end{array} \right]_{3 \times P_y} \hat{T}_y = B_y \hat{T}_y. \end{aligned} \tag{13}$$

Case III - only $\hat{T}_z \neq 0$, that is, $\hat{T}_x = \hat{T}_y = 0$. From (11),

$$\begin{aligned} \hat{T}(x) &= \hat{T}_n(x) = T_x T_y \hat{T}_z = [T_x T_y \Phi_z]_{1 \times P_z} \hat{T}_z = N_z \hat{T}_z, \\ \delta \nabla T &= \left[\begin{array}{c} T_{x,x} T_y \Phi_z \\ T_x T_{y,y} \Phi_z \\ T_x T_y \Phi_{z,z} \end{array} \right]_{3 \times P_z} \hat{T}_z = B_z \hat{T}_z. \end{aligned} \tag{14}$$

2.1 Weak forms

2.1.1 Case I - only $\hat{T}_x \neq 0$, given $T_y(y)$ and $T_z(z)$

From (7), the approximate temperature at the new mode n is in the form

$$\begin{aligned} T(x) &= T_0(x) + [T_y \; T_z \; \Phi_x] T_x, \\ &= T_0(x) + N_x T_x. \end{aligned}$$

and the gradient,

$$\nabla T = \nabla T_0 + \left[\begin{array}{c} T_y T_z \Phi_{x,x} \\ T_{y,y} T_z \Phi_x \\ T_y T_{z,z} \Phi_x \end{array} \right]_{3\times P_x} T_x = \nabla T_0 + B_x T_x. \tag{15}$$

The approximate weak form (3) becomes

$$\hat{T}_x^T \left(\int_\Omega k B_x^T B_x d\Omega \right) T_x = \hat{T}_x^T \left(\int_\Omega N_x^T b \, d\Omega + \int_{\Gamma_q} N_x^T h \, d\Omega - \int_\Omega k B_x^T \nabla T_0 d\Omega - \int_\Omega k B_x^T \nabla G d\Omega \right) \tag{16}$$

that is, $K_x T_x = F_x$, where K_x has dimensions $P_x \times P_x$.

2.1.2 Case II - only $\hat{T}_y \neq 0$, given $T_x(y)$ and $T_z(z)$

Using expressions analogous to (15), gives

$$\begin{aligned} T(x) &= T_0(x) + [T_x \; T_z \; \Phi_y] T_y, \\ &= T_0(x) + N_y T_y. \end{aligned}$$

and the gradient,

$$\nabla T = \nabla T_0 + \left[\begin{array}{c} T_{x,x} T_z \Phi_y \\ T_x T_z \Phi_{y,y} \\ T_x T_{z,z} \Phi_y \end{array} \right]_{3\times P_x} T_y = \nabla T_0 + B_y T_y. \tag{17}$$

the weak form (3) becomes

$$\hat{T}_y^T \left(\int_\Omega k B_y^T B_y \right) T_y = \hat{T}_y^T \left(\int_\Omega N_y^T b + \int_{\Gamma_q} N_y^T h \, d\Omega - \int_\Omega k B_y^T \nabla T_0 d\Omega - \int_\Omega k B_y^T \nabla G d\Omega \right) \tag{18}$$

that is, $K_y T_y = F_y$, where K_y has dimensions $P_y \times P_y$.

Analogously, for the case III, where only $\hat{T}_z \neq 0$, given $T_x(y)$ and $T_y(z)$, the weak form (3) becomes (with $T(x) = T_0(x) + [T_x \; T_y \; \Phi_z] T_z$)

$$\hat{T}_z^T \left(\int_\Omega k B_z^T B_z \right) T_z = \hat{T}_z^T \left(\int_\Omega N_z^T b + \int_{\Gamma_q} N_z^T h \, d\Omega - \int_\Omega k B_z^T \nabla T_0 d\Omega - \int_\Omega k B_z^T \nabla G d\Omega \right) \tag{19}$$

that is, $K_z T_z = F_z$, where K_z has dimensions $P_z \times P_z$.

2.2 Separation of integration in the stiffness matrices

Taking the stiffness matrix from eq.(16), and taking the composition of B_x from (12) we have

$$\begin{aligned} K_x &= \int_\Omega k B_x^T B_x d\Omega, \\ &= \int_\Omega \left(k T_y^2 T_z^2 \Phi_{x,x}^T \Phi_{x,x} + k T_{y,y}^2 T_z^2 \Phi_x^T \Phi_x + k T_y^2 T_{z,z}^2 \Phi_x^T \Phi_x \right) d\Omega, \end{aligned} \tag{20}$$

and introducing the PGD decomposition of k from (5), we will obtain K_x as summation:

$$K_x = \sum_{l=1}^{nk} D_l K_x^l \tag{21}$$

where

$$\begin{aligned} K_x^l &= \left(\int_x k_{xl}\Phi_{x,x}^T\Phi_{x,x}\,dx\right)\left(\int_y k_{yl}T_y^2\,dy\right)\left(\int_z k_{zl}T_z^2\,dz\right) \\ &+ \left(\int_x k_{xl}\Phi_x^T\Phi_x\,dx\right)\left(\int_y k_{yl}T_{y,y}^2\,dy\right)\left(\int_z k_{zl}T_z^2\,dz\right) \\ &+ \left(\int_x k_{xl}\Phi_{x,x}^T\Phi_{x,x}\,dx\right)\left(\int_y k_{yl}T_y^2\,dy\right)\left(\int_z k_{zl}T_{z,z}^2\,dz\right) \end{aligned} \tag{22}$$

Analogously, we have

$$K_y^l = \sum_{l=1}^{nk} D_l K_y^l \quad \text{and} \quad K_z^l = \sum_{l=1}^{nk} D_l K_z^l, \tag{23}$$

where

$$\begin{aligned} K_y^l &= \left(\int_x k_{xl}T_{x,x}^2\,dx\right)\left(\int_y k_{yl}\Phi_y^T\Phi_y\,dy\right)\left(\int_z k_{zl}T_z^2\,dz\right) \\ &+ \left(\int_x k_{xl}T_x^2\,dx\right)\left(\int_y k_{yl}\Phi_{y,y}^T\Phi_{y,y}\,dy\right)\left(\int_z k_{zl}T_z^2\,dz\right) \\ &+ \left(\int_x k_{xl}T_x^2\,dx\right)\left(\int_y k_{yl}\Phi_y^T\Phi_y\,dy\right)\left(\int_z k_{zl}T_{z,z}^2\,dz\right) \end{aligned} \tag{24}$$

and

$$\begin{aligned} K_z^l &= \left(\int_x k_{xl}T_{x,x}^2\,dx\right)\left(\int_y k_{yl}T_y^2\,dy\right)\left(\int_z k_{zl}\Phi_z^T\Phi_z\,dz\right) \\ &+ \left(\int_x k_{xl}T_x^2\,dx\right)\left(\int_y k_{yl}T_{y,y}^2\,dy\right)\left(\int_z k_{zl}\Phi_z^T\Phi_z\,dz\right) \\ &+ \left(\int_x k_{xl}T_x^2\,dx\right)\left(\int_y k_{yl}T_y^2\,dy\right)\left(\int_z k_{zl}\Phi_{z,z}^T\Phi_{z,z}\,dz\right). \end{aligned} \tag{25}$$

3. Generation of PGD representation of data

Consider a scalar material property, like thermal conductivity component $k_{ij}(x)$, (or elastic modulus component $E_{ij}(x)$) or thermal source $b(x)$, heat flux at a region of the boundary $h(x)$, etc. Consider its variation on the domain highly oscillatory or random, as in an heterogeneous non-periodical material. Consider a PGD representation for $k(x)$:

$$\tilde{k}(x) = \underbrace{\sum_{l=1}^{nk} D_l k_{xl}(x) k_{yl}(y) k_{zl}(z)}_{k_0(x)} + \underbrace{k_x(x) k_y(y) k_z(z)}_{k_n(x)}, \quad \text{that is, } \tilde{k}(x) = k_0(x) + k_n(x). \tag{26}$$

where $k_0(x)$ is known and we seek $k_n(x)$. The coefficients D_l are determined in a second step of the method. In the first step, it is considered known, generally arbitrated as unitary. We define a squared error functional as

$$E(k_x, k_y, k_z) = \int_\Omega \left[k(x) - (k_0 + k_x k_y k_z)\right]^2 \, d\Omega. \tag{27}$$

where $k(x)$ is the given data of the property. The variations of the error functional are

$$\begin{aligned}
\delta E_x(k_x, k_y, k_z) &= \frac{\partial E}{\partial k_x} \delta k_x = 2 \int_\Omega \left[k(x) - \tilde{k}\right] \delta k_x k_y k_z \, d\Omega = 0, \\
\delta E_y(k_x, k_y, k_z) &= \frac{\partial E}{\partial k_y} \delta k_y = 2 \int_\Omega \left[k(x) - \tilde{k}\right] \delta k_y k_x k_z \, d\Omega = 0, \\
\delta E_z(k_x, k_y, k_z) &= \frac{\partial E}{\partial k_z} \delta k_z = 2 \int_\Omega \left[k(x) - \tilde{k}\right] \delta k_z k_x k_y \, d\Omega = 0,
\end{aligned} \tag{28}$$

We proceed to a **spatial discretization** for $k_n(x)$:

$$\begin{aligned}
k_x(x) &= \sum_{p=1}^{nx} Q_{xp} \phi_{xp}(x) = \Phi_x(x) Q_x, \\
k_y(y) &= \sum_{p=1}^{ny} Q_{yp} \phi_{yp}(y) = \Phi_y(y) Q_y, \\
k_z(z) &= \sum_{p=1}^{nz} Q_{zp} \phi_{zp}(z) = \Phi_z(z) Q_z.
\end{aligned} \tag{29}$$

where Q_x, Q_y and Q_z are row vectors of nodal values of the approximation. Eq.$(28)_1$ gives

$$\int_\Omega \left[k(x) - k_0\right] k_y k_z \delta k_x \, d\Omega = \int_\Omega k_x k_y^2 k_z^2 \delta k_x \, d\Omega. \tag{30}$$

The variation δk_x is represented from $(29)_1$

$$\delta k_x = \Phi_x(x) \hat{Q}_x. \tag{31}$$

Thus, (30) becomes

$$\hat{Q}_x^T \underbrace{\int_\Omega \Phi_x^T \left[k(x) - k_0\right] k_y k_z \, d\Omega}_{F_x} = \hat{Q}_x^T \underbrace{\left[\int_x \Phi_x^T \Phi_x dx \int_y k_y^2 dy \int_z k_z^2 \, dz\right]}_{K_x} Q_x, \tag{32}$$

$$K_x Q_x = F_x, \tag{33}$$

where K_x is a symmetric mass-matrix like, which is obtained from three independent 1D integrals. However, at this point, F_x requires coupled integration in all three dimensions, due to the physical data $k(x)$.

Analogously, we obtain y and z systems:

$$K_y Q_y = F_y \qquad \text{and} \qquad K_z Q_z = F_z, \tag{34}$$

where

$$\begin{array}{ll} K_y = \int_x k_x^2\, dx \int_y \Phi_y^T \Phi_y\, dy \int_z k_z^2\, dz & F_y = \int_\Omega \Phi_y^T\, [k(x) - k_0]\, k_x k_z\, d\Omega, \\ K_z = \int_x k_x^2\, dx \int_y k_y^2\, dy \int_z \Phi_z^T \Phi_z\, dz & F_z = \int_\Omega \Phi_z^T\, [k(x) - k_0]\, k_x k_y\, d\Omega. \end{array} \tag{35}$$

Algebraic systems (33)-(34) are coupled and nonlinear. Their solution can be done using the successive iteration method.

The force term in (32) can be decomposed using the PGD separated representation of $k_0 = \sum_{l=1}^{nk} D_l\, k_{xl}(x)\, k_{yl}(y)\, k_{zl}(z)$:

$$\begin{aligned} F_x &= \int_\Omega \Phi_x^T\, [k(x) - k_0]\, k_y k_z\, d\Omega, \\ &= \int_\Omega \Phi_x^T k(x) k_y k_z\, d\Omega - \int_\Omega \Phi_x^T k_0 k_y k_z\, d\Omega, \\ &= \int_\Omega \Phi_x^T k(x) k_y k_z\, d\Omega - \sum_{l=1}^{nk} D_l \left(\int_x \Phi_x^T k_{xl}\, dx \right) \left(\int_y k_{yl} k_y\, dy \right) \left(\int_z k_{zl} k_z\, dz \right), \\ &= \int_\Omega \Phi_x^T k(x) k_y k_z\, d\Omega - \sum_{l=1}^{nk} F_x^l \\ &= F_x^k - F_x^0. \end{aligned} \tag{36}$$

Analougously,

$$\begin{aligned} F_y &= \int_\Omega \Phi_y^T k(x) k_x k_z\, d\Omega - \sum_{l=1}^{nk} D_l \left(\int_x k_{xl} k_x\, dx \right) \left(\int_y \Phi_y^T k_{yl}\, dy \right) \left(\int_z k_{zl} k_z\, dz \right), \\ F_z &= \int_\Omega \Phi_z^T k(x) k_x k_y\, d\Omega - \sum_{l=1}^{nk} D_l \left(\int_x k_{xl} k_x\, dx \right) \left(\int_y k_{yl}^2\, dy \right) \left(\int_z \Phi_z^T k_{zl}\, dz \right), \end{aligned} \tag{37}$$

that is,

$$F_y = F_y^k - F_y^0 \qquad \text{and} \qquad F_z = F_z^k - F_z^0. \tag{38}$$

Therefore, the parts F_x^0, F_y^0 and F_z^0 can be integrated separately in each direction, and only F_x^k, F_y^k and F_z^k must be integrated in coupled form.

3.1 Data generation for tests

We consider here two types of property data for use in the PGD tests: continuous harmonic functions and a two phase material (which gives a discontinuous property distribution). Both forms can be made random or can generate properties with sharp gradients.

3.1.1 Harmonic variation

We consider the following description

$$k(x) = \sum_{m=1}^{nm} \left(A_m \sin\frac{i_m \pi x}{L_x} \sin\frac{j_m \pi y}{L_y} \sin\frac{k_m \pi z}{L_z} + B_m \cos\frac{i_m \pi x}{L_x} \cos\frac{j_m \pi y}{L_y} \cos\frac{k_m \pi z}{L_z} \right), \tag{39}$$

with m, i_m, j_m, $k_m \in \mathbb{N}$, and L_x, L_y, $L_z \in \mathbb{R}$, are the dimensions of the domain. A_m, B_m and i_m, j_m, k_m can be arbitrated or obtained from a generator of random numbers.

This representation has uncoupled coordinates. Substituting it in $F_x^k = \int_\Omega \Phi_x^T k(x) k_y k_z \, d\Omega$ of (36) one obtain

$$\begin{aligned} F_x^k \;=\; & \sum_{m=1}^{nm} A_m \left(\int_x \Phi_x^T \sin\frac{i_m \pi x}{L_x} dx \right) \left(\int_y k_y \sin\frac{j_m \pi y}{L_y} dy \right) \left(\int_z k_z \sin\frac{k_m \pi z}{L_z} dz \right) + \\ & \sum_{m=1}^{nm} B_m \left(\int_x \Phi_x^T \cos\frac{i_m \pi x}{L_x} dx \right) \left(\int_y k_y \cos\frac{j_m \pi y}{L_y} dy \right) \left(\int_z k_z \cos\frac{k_m \pi z}{L_z} \, dz \right), \end{aligned} \tag{40}$$

and analogously,

$$\begin{aligned} F_y^k \;=\; & \sum_{m=1}^{nm} A_m \left(\int_x \sin\frac{i_m \pi x}{L_x} dx \right) \left(\int_y \Phi_y^T k_y \sin\frac{j_m \pi y}{L_y} dy \right) \left(\int_z k_z \sin\frac{k_m \pi z}{L_z} dz \right) + \\ & \sum_{m=1}^{nm} B_m \left(\int_x \cos\frac{i_m \pi x}{L_x} dx \right) \left(\int_y \Phi_y^T k_y \cos\frac{j_m \pi y}{L_y} dy \right) \left(\int_z k_z \cos\frac{k_m \pi z}{L_z} \, dz \right), \end{aligned} \tag{41}$$

$$\begin{aligned} F_z^k \;=\; & \sum_{m=1}^{nm} A_m \left(\int_x \sin\frac{i_m \pi x}{L_x} dx \right) \left(\int_y k_y \sin\frac{j_m \pi y}{L_y} dy \right) \left(\int_z \Phi_z^T k_z \sin\frac{k_m \pi z}{L_z} dz \right) + \\ & \sum_{m=1}^{nm} B_m \left(\int_x \cos\frac{i_m \pi x}{L_x} dx \right) \left(\int_y k_y \cos\frac{j_m \pi y}{L_y} dy \right) \left(\int_z \Phi_z^T k_z \cos\frac{k_m \pi z}{L_z} \, dz \right). \end{aligned} \tag{42}$$

3.1.2 Power variation

We consider the following description

$$k(x) = \sum_{m=1}^{nm} A_m \, x^{i_m} \, y^{j_m} \, z^{k_m}, \tag{43}$$

with m, i_m, j_m, $k_m \in \mathbb{N}$. A_m and i_m, j_m, k_m can be arbitrated or obtained from a generator of random numbers.

This representation has uncoupled coordinates. Substituting it in $F_x^k = \int_\Omega \Phi_x^T k(x) k_y k_z \, d\Omega$ of (36) one obtain

$$F_x^k = \sum_{m=1}^{nm} A_m \left(\int_x \Phi_x^T x^{i_m} \, dx \right) \left(\int_y k_y y^{j_m} \, dy \right) \left(\int_z k_z z^{k_m} \, dz \right), \tag{44}$$

and similarly for F_y^k and F_z^k.

3.1.3 Two phase material

Consider the heterogeneous material constituted by a matrix of property k^m and inclusions of property k^i. Both matrix and inclusions are considered isotropic homogeneous. Consider that each inclusion p has its geometric center located at coordinate x_p and be spherical or cubic with radius/side r_p as illustrated in Figure 1. To simplify the subsequent use, the cubic inclusion is restricted here to the case where its sides are parallel to the global Cartesian axes. Consider that both position and dimension be randomly determined. In this way, it is possible partial or total superposition of inclusions. One possible way to avoid that consists in post-processing the data, testing each pair of inclusions and eliminating those in partial or total superposition.

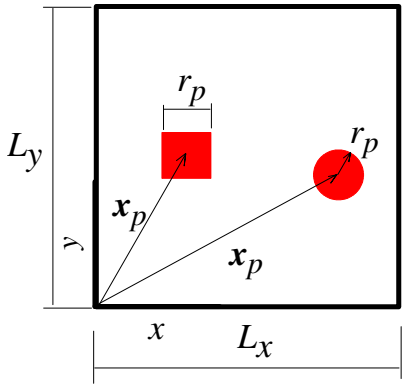

Figure 1. Heterogeneous material with inclusions.

Let us consider the property of the inclusion be decomposed as

$$k^i = k^m + \Delta k. \tag{45}$$

Thus, $F_x^k = \int_\Omega Q_x^T k(x) k_y k_z \, d\Omega$ of (36) becomes

$$F_x^k = k^m \int_\Omega \Phi_x^T k_y k_z \, d\Omega + \Delta k \int_{\Omega_i} \Phi_x^T k_y k_z \, d\Omega \tag{46}$$

where Ω_i is the union of the inclusion domains. k^m is a constant in Ω and Δk is constant in every inclusion. If the inclusion is cubic with faces parallel to the coordinate axes, both integrals can be uncoupled in the Cartesian directions:

$$F_x^k = k^m \int_x \Phi_x^T \, dx \int_y k_y \, dy \int_z k_z \, dz + \Delta k \sum_{p=1}^{ni} \int_{x \in \Omega_p} \Phi_x^T dx \int_{y \in \Omega_p} k_y dy \int_{z \in \Omega_p} k_z \, dz \tag{47}$$

ni is the number of inclusions and Ω_p is the domain of the p-th inclusion. Analogously,

$$F_y^k = k^m \int_x k_x\, dx \int_y \Phi_y^T\, dy \int_z k_z\, dz + \Delta k \sum_{p=1}^{ni} \int_{x\in\Omega_p} k_x dx \int_{y\in\Omega_i} \Phi_y^T dy \int_{z\in\Omega_p} k_z\, dz$$

$$F_z^k = k^m \int_x k_x\, dx \int_y k_y\, dy \int_z \Phi_z^T\, dz + \Delta k \sum_{p=1}^{ni} \int_{x\in\Omega_p} k_x dx \int_{y\in\Omega_p} k_y dy \int_{z\in\Omega_p} \Phi_z^T\, dz \tag{48}$$

In this way, in tests for the PGD representation, all integrals can be uncoupled in the Cartesian directions if the data are generated from harmonic or two phase materials. However, for a real material, the force vectors in (36) will have to be obtained by coupled 3D integrals.

3.2 Determination of the amplitudes of the data modes

Let us consider that, at a given point, one has a set of nk modes $k_{xl}(x)k_{yl}(y)k_{zl}(z)$. Each function $k_{xl}(x)$, $k_{yl}(y)$, etc., can have been normalized by its maximum value or not. At this step, it is useful generate a new determination of the entire set of coefficient D_l, given the modes fixed, that is, determine D_l such that

$$\tilde{k}(x) = \sum_{l=1}^{nk} D_l k_{xl}(x)k_{yl}(y)k_{zl}(z) \tag{49}$$

improves the approximation of the given function $k(x)$. Therefore, we define the error functional as

$$E(D_l) = \int_\Omega \left[k(x) - \sum_{l=1}^{nk} D_l k_{xl}(x)k_{yl}(y)k_{zl}(z) \right]^2 d\Omega. \tag{50}$$

The variation of the error in relation to D_s generates

$$\underbrace{\int_\Omega k(x)k_{xs}(x)k_{ys}(y)k_{zs}(z)d\Omega}_{G_s} = \sum_{l=1}^{nk} \underbrace{\left(\int_x k_{xs}k_{xl}dx \int_y k_{ys}k_{yl}(y)dy \int_z k_{zs}k_{zl}(z)dz \right)}_{C_{sl}} D_l, \tag{51}$$

for $s,l = 1,nk$. This produces the algebraic system

$$CD = G \tag{52}$$

where C is a nk square symmetric matrix. The force term depends on the data. In case of the generated harmonic data (39), it can be integrated separately as

$$\begin{aligned} G_s &= \int_\Omega k(x)k_{xs}(x)k_{ys}(y)k_{zs}(z)\, d\Omega, \\ &= \sum_{m=1}^{nm} A_m \int_x k_{xs} \sin\frac{i_m\pi x}{L_x} dx \int_y k_{ys} \sin\frac{j_m\pi y}{L_y} dy \int_z k_{zs} \sin\frac{k_m\pi z}{L_z} dz + \\ &\sum_{m=1}^{nm} B_m \int_x k_{xs} \cos\frac{i_m\pi x}{L_x} dx \int_y k_{ys} \cos\frac{j_m\pi y}{L_y} dy \int_z k_{zs} \cos\frac{k_m\pi z}{L_z} dz. \end{aligned} \tag{53}$$

4. Numerical results

Let us consider a two dimensional VRE of dimensions $L_x = L_y = 10$ and arbitrate two simple descriptions for the k constant: the trigonometric and the power ones, with the following parameters: $A_1 = 3$, $i_1 = 2$, $j_1 = 1$, $A_2 = 3$, $i_2 = 2$, $j_2 = 2$. All $B_m = 0$. In this way, the data are generated according to

$$\begin{aligned} &\text{Data 1: } k(x) = 3\sin\frac{2\pi x}{L_x}\sin\frac{\pi y}{L_y} + 3\sin\frac{2\pi x}{L_x}\sin\frac{2\pi y}{L_y} \quad \text{and} \\ &\text{Data 2: } k(x) = 3\,x^2\,y + 3\,x^2\,y^2. \end{aligned} \tag{54}$$

PGD approximates both functions with only one mode. We fixed 19 nodes equally spaced in each direction. The functions $k_x(x)$ and $k_y(y)$ associated to the first PGD mode are shown in Figures 2 and 3. Their product generate the PGD approximation for the data, which are shown in Figures 4 and

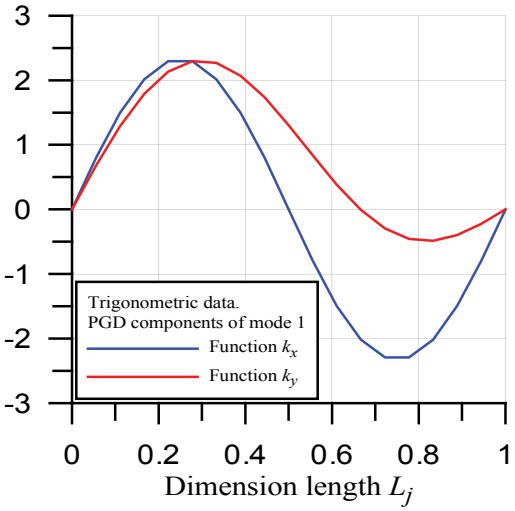

Figure 2. Functions for the PGD mode 1 for trigonometric data 1.

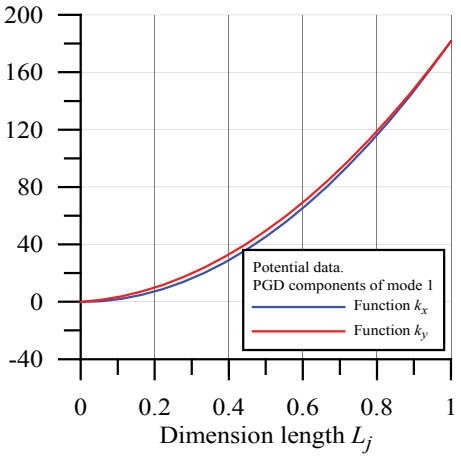

Figure 3. Functions for the PGD mode 1 for potential data 2.

5. The pointwise error with respect to the exact data of (54) are shown in Figures 6 and 7. For the potential data, the relative error at the maximum point of the data, is about 0,1 %. One notice that the

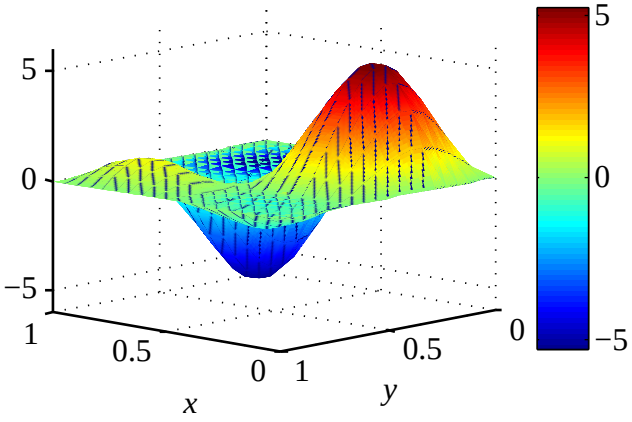

Figure 4. PGD approximation for trigonometric data 1.

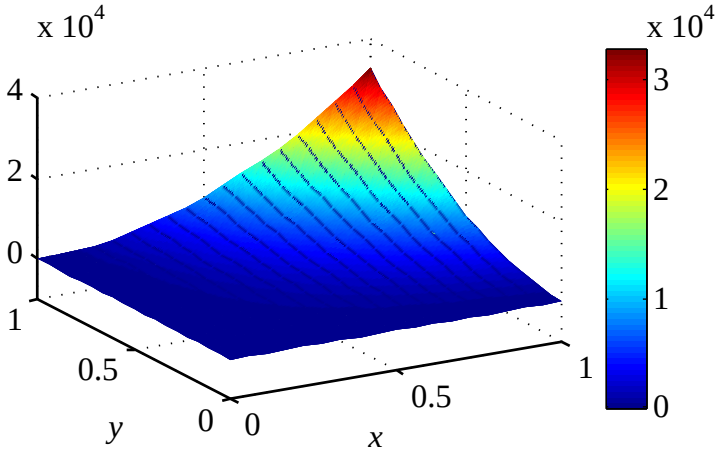

Figure 5. PGD approximation for potential data 2.

figures were obtained with a grid of 19×19 points, that is, it takes $19^2 = 361$ points of information. In fact, the PGD representation requires only $2 \times 19 = 38$ values. In three dimensions this would be $19^3 = 6869$ versus $3 \times 19 = 57$ values to store the same information.

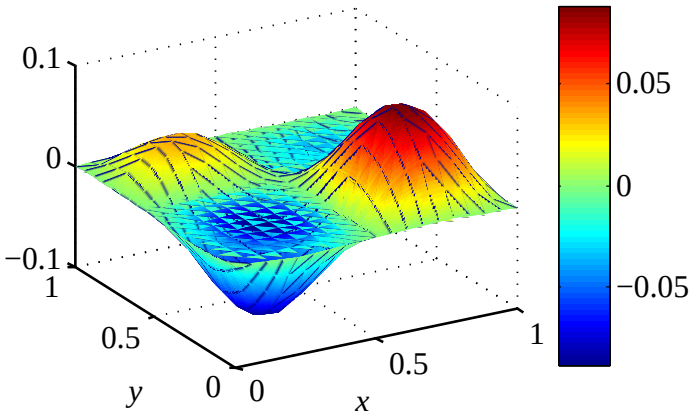

Figure 6. Error between PGD approximation and exact trigonometric data 1.

Next we consider a heterogeneous material with a square inclusion. Using the notation of Figure 1, its center is located at $x = y = 5$ mm and its length is 4 mm. The material has properties $k^m = 1$ $W \cdot (m \cdot K)^{-1}$ and $\Delta k = 4\, W \cdot (m \cdot K)^{-1}$. The exact solution for this material is shown in Figure 8, made

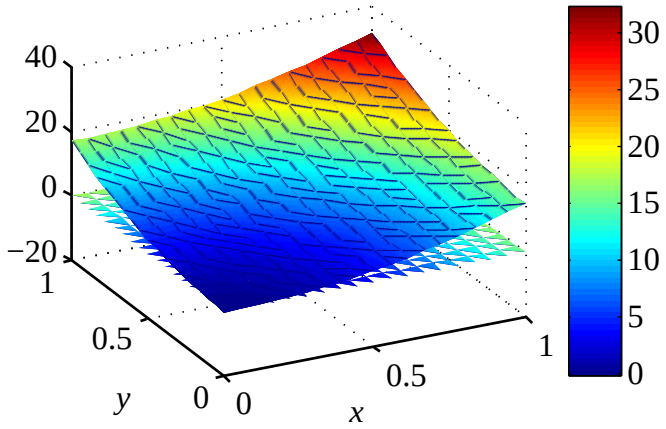

Figure 7. Error between PGD approximation and exact potential data 2.

with 50x50 for visualization, because of that the sides of the inclusion seems to have an inclination, but actually its a complete vertical as can be seen in Figure 9.

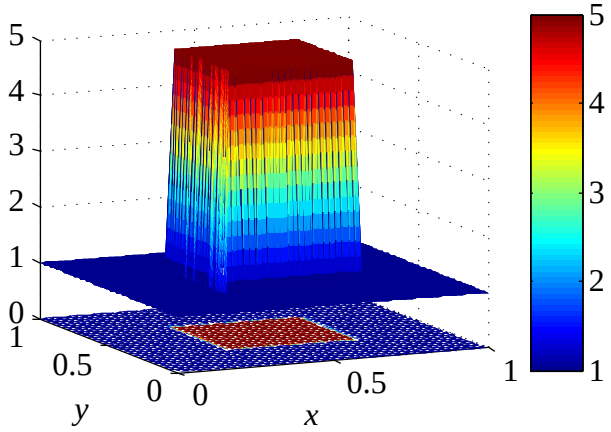

Figure 8. Exact solution for heterogeneous material with square inclusion

For this case, we fixed four different quantities of elements, equally spaced, for each direction: 10, 20, 50 and 200. Using convergence tolerance, maximum number of modes and points of integration of 10^{-6}, 6 and 2, respectively. The PGD approximates the solution with 2 modes for the cases with 10 and 20 elements and with 3 modes for 50 and 200. The PGD solution for all cases and the exact solution are shown in Figure 9 along an axis at coordinate x or $y = 5$ mm, one may notice that as the inclusion is a square, both solutions in x or y are the same.

The pointwise relative errors, using (55), for all quantities of elements are shown in Figure 10. The relative error gets its maximum in the discontinuity between the normal material and the inclusion, which takes around 50 %.

$$E(\mathbf{x}) = \left| \frac{k(\mathbf{x}) - k_{exact}(\mathbf{x})}{k_{exact}(\mathbf{x})} \right| \tag{55}$$

The product between the solution, for 50x50, generates the grid shown in Figure 11, made with 309 points of information. One may notice that the solution in the figure is shown just the first quarter for better visualization, but as the inclusion is a square in the center, the solution becomes symmetric.

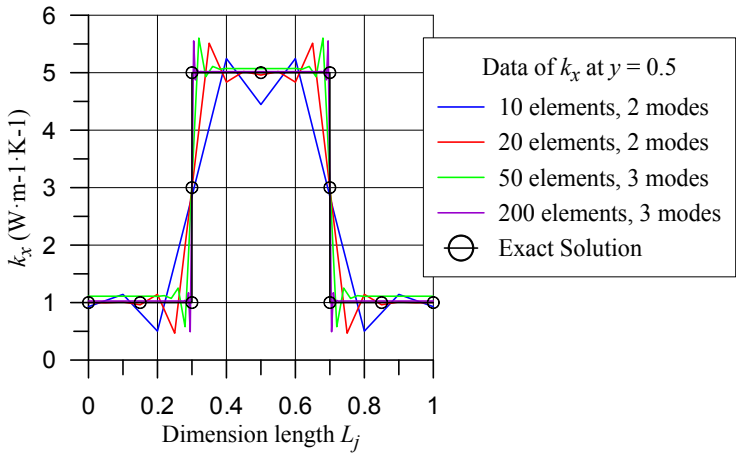

Figure 9. PGD functions for heterogeneous material with square inclusion

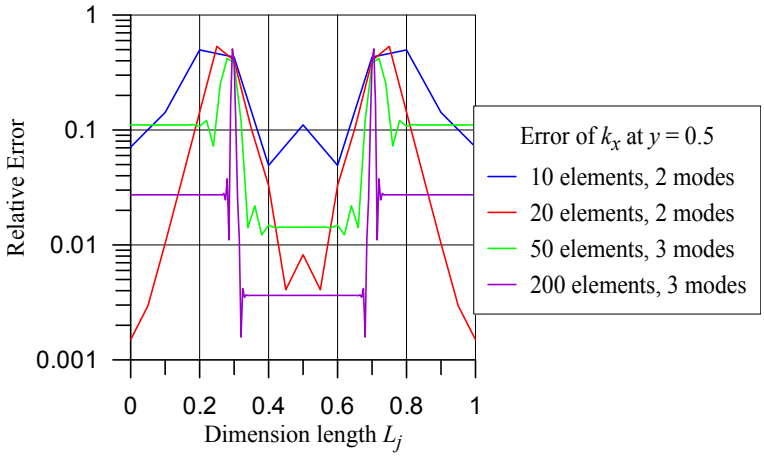

Figure 10. Error between functions of PGD approximation and exact solution for heterogeneous material with square inclusion

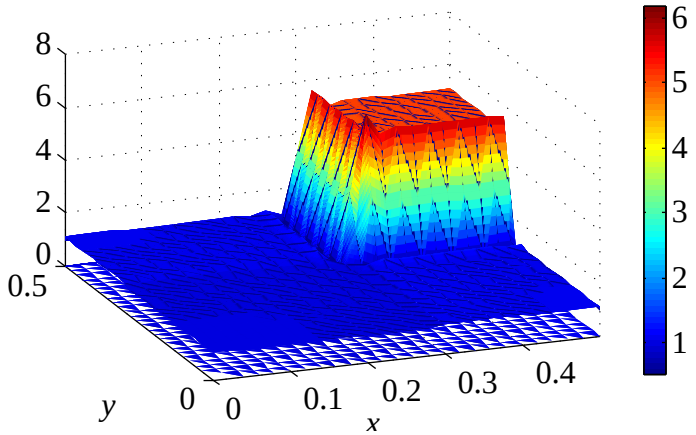

Figure 11. PGD approximation for heterogeneous material with square inclusion

5. CONCLUSIONS

A PGD formulation was developed to obtain a PGD description of a highly oscillatory local material property data. This description is composed by a sequence of discrete modes uncoupled in each of the three Cartesian coordinates. The tests were shown for the conductivity constant in a isotropic material, but the same procedure is equally applicable to each individual component of the tensor

of conductivity constants in an anisotropic material. Also, the same technique is used to create a PGD representation of all data necessary to the PGD modeling of the heat transfer problem. In fact, prior to this modeling, it is necessary to generate PGD representations for temperature and heat flux prescribed in each of the faces of the RVE.

The results obtained so far indicate that the PGD technique is capable of generating data representation with great accuracy and efficiesncy, and can be used to represent data in RVE obtained from physical samples of different materials.

REFERENCES

[1] Hori, M., Nemat-Nasser, S. (1999) On Two Micromechanics Theories for Determining Micro-Macro Relations in Heterogeneous Solids, Mech. of Materials, 31:667-682.

[2] Michel, J.C., Moulinec, H., Suquet, P. (1999), Efective Properties of Composite Materials with Periodic Microstructure: A Computational Approach, Comp. Meth. Appl. Mech. Engng., 172:109-143.

[3] Nemat-Nasser, S. (1999) Averaging Theorems in Finite Deformation Plasticity, Mech. Materials, 31:493-523.

[4] Miehe, C., Shotte, J. & Lambrecht, M. (2002) Homogenization of Inelastic Solid Materials at Finite Strains Based on Incremental Minimization Principles. Application to the Texture Analysis of Polycrystals, J. Mech. Phys. Solids, 50(10):2123-2167.

[5] Clayton, J.D., McDowell, D.L. (2003) A Multiscale Multiplicative Decomposition for Elastoplasticity of Polycrystals, Int. J. of Plasticity, 19:1401-1444.

[6] Ibrahimbegovic, A., Markovi c, D. (2003) Strong Coupling Methods in Multi-Phase and Multi-Scale Modeling of Inelastic Behavior of Heterogeneous Structures, Comp. Meth. Appl. Mech. Engng., 192:3089-3107.

[7] Miehe, C. (2002) Strain-Driven Homogenization of Inelastic Microstructures and Composites Based on an Incremental Variational Formulation, Int. J. Num.Meth. Engng., 55:1285-1322.

[8] Miehe, C. and Koch, A. (2002), Computational Micro-to-Macro Transitions of Discretized Microstructures Undergoing Small Strains, Arch. Appl. Mech.,72:300-317.

[9] Miehe, C. (2003), Computational Micro-to-Macro Transitions for Discretized Micro-Structures of Heterogeneous Materials at Finite Strains Based on the Minimization of Averaged Incremental Energy, Comp. Meth. Appl. Mech.Engng., 192:559-591.

[10] Reese, S. (2003) Meso-Macro Modelling of Fibre-Reinforced Rubber-Like Composites Exhibiting Large Elastoplastic Deformations, Int. J. Solids Struct.,40:951-980.

[11] Terada, K., Saiki, I., Matsui, K., Yamakawa, Y. (2003) Two-Scale Kinematcs and Linearization for Simultaneous Two-Scale Analysis of Periodic Heterogeneous Solids at Finite Strains, Comp. Meth. Appl. Mech. Engng., 192:3531-3563.

[12] DVORKIN M., ARMBRUSTER,C. The future of rock physics: computational methods vs. lab testing. *First Break*, v. 8, p. 6, 2008.

[13] KETCHAM, R. A., CARLSON, W. D. Acquisition, optimization and interpretation of x-ray computed tomographic imagery: Applications to the geosciences. *Comput. Geosci.*, Pergamon Press, Inc., Tarrytown, NY. v. 27, n. 4, p. 381–400, maio 2001. ISSN 0098-3004.

[14] GARBOCZI, E. J. Finite Element and Finite Difference Programs for Computing the Linear Electric and Elastic Properties of Digital Images of Random Materials. [S.l.], December 1998.

[15] NETO, E. A. d. S., Feijóo, R. A. Variational Foundations of Multi-Scale Constitutive Models of Solid: Small and Large Strain Kinematical Formulation. 11 2006. *LNCC R&D Report*.

[16] ARNS, C. H.; KNACKSTEDT, M. A., PINCZEWSKI, W. V., GARBOCZI, E. J. Computation of linear elastic properties from microtomographic images: Methodology and agreement between theory and experiment. Geophysics, SEG, v. 67, n. 5, p. 1396–1405, 2002.

[17] Hassani, B., Hinton, E. *Homogenization and Structural Topology Optimization: Theory, Practice, and Software*. Springer, 1999. ISBN 9783540762119.

[18] B. Bognet, F. Bordeu, F. Chinesta, A. Leygue, A. Poitou, Advanced simulation of models defined in plate geometries: 3D solutions with 2D computational complexity, *Comput. Methods Appl. Mech. Engrg*. 201–204, 2012, p. 1–12.

[19] N. Anthony, A prior model reduction through Proper Generalized Decomposition for solving time-dependent partial differential equations, *Comput. Methods Appl. Mech. Engrg*. 198, 2010, p. 1603-1626.

[20] D. González, A. Ammar, F. Chinesta, E. Cueto, Recent advances on the use of separated representations, *Int. J. Numer. Meth. Engng* 2010; 81:637–659.

RESPONSIBILITY NOTICE

The authors are the only responsible for the printed material included in this paper.